

**NUMERICAL INVESTIGATION ON THE EFFECTS
OF GEOMETRICAL PARAMETERS ON FILM
COOLING PERFORMANCE**

AMIR HUSSEIN ALI

UNIVERSITI SAINS MALAYSIA

2013

**NUMERICAL INVESTIGATION ON THE EFFECTS
OF GEOMETRICAL PARAMETERS ON FILM
COOLING PERFORMANCE**

By

AMIR HUSSEIN ALI

**Thesis Submitted to the School of Mechanical Engineering
in Fulfillment of the Requirements
for the Degree of Doctor of Philosophy in Mechanical Engineering**

July 2013

ACKNOWLEDGEMENTS

The first thank is to Allah for helping me in performing my PhD degree.

Special thanks to my supervisors, Dr. Nadiahnor Binti Md. Yusop (main supervisor) and Professor Dr. Mohd Zulkifly Abdullah (co-supervisor) for their help, suggestions, consistent supervision during the period of the study.

My appreciation is also extended to Universiti Sains Malaysia, Institute of Postgraduate Studies. Also my thanks to the Dean, Deputy Deans, lecturers and all technical staff of School of Mechanical Engineering and Aerospace Engineering, (USM).

My greatest gratitude and appreciations are to my mother, all of my brothers and all of my sisters.

Finally, this work has been dedicated to my father's spirit.

AMIR HUSSEIN ALI

TABLE OF CONTENTS

	Page
ACKNOWLEDGEMENTS	ii
TABLE OF CONTENTS	iii
LIST OF TABLES	viii
LIST OF FIGURES	ix
LIST OF SYMBOLS	xx
ABSTRAK	xxiv
ABSTRACT	xxvi
CHAPTER 1: INTRODUCTION	
1.1 Film Cooling	1
1.2 Film cooling fundamentals	5
1.2.1 Film cooling effectiveness	7
1.2.2 Conjugate film cooling	7
1.2.3 Computational fluid dynamic (CFD) for effectiveness prediction	8
1.3 Problem Statement	11
1.4 Objectives	12
1.5 Scope of the work	13

1.6 Overview of the thesis	14
CHAPTER 2: LITERATURE REVIEW	
2.1 Introduction	15
2.2 Effect of film cooling geometry on film cooling effectiveness, η	15
2.3 Effect of physical parameters on film cooling effectiveness, η	42
2.4 Effect of surface curvature on film cooling effectiveness, η	52
2.5 conjugate heat transfer and film cooling effectiveness	64
CHAPTER 3: METHODOLOGY	
3.1 Introduction	70
3.2 Numerical methodology	71
3.2.1 Mathematical equations	71
3.2.1.a Turbulent mass and momentum flow equations	71
3.2.1.b Energy equations	72
3.2.2 Turbulence models	73
3.2.2.a Transport equations for kinetic equation	74
3.2.2.b Dissipation rate	74
3.3 Computational methodology	74
3.3.1 Discretization method	75
3.3.2 Validation	76

3.3.2.a	Boundary conditions of the validation study	76
3.3.2.b	Grid independence and mesh examination	78
3.4	Adiabatic methodology	81
3.4.1	Computational investigation for diffused and compound cooling holes	81
3.4.2	New anti-vortex scheme (heart-shaped) for film-cooling hole	84
3.4.2.a	Heart-shaped cooling hole theory	84
3.4.2.b	Heart-shaped boundary conditions and computational methods	88
3.5	Conjugate film cooling and heat transfer studies	90
3.5.1	Conjugate film cooling of new multi-layers convex surface	90
3.5.1.a	Multi-layers convex surface theory	92
3.5.1.b	Multi-layers convex surface boundary conditions	93
3.5.2	Conjugate film cooling of staggered distribution	95
3.5.3	Conjugate film cooling of heart-shaped cooling hole	97
 CHAPTER 4: RESULTS AND DISCUSSION		
4.1	Introduction	103
4.2	Grid independence and validation study	103
4.2.1	Meshing type investigation	104
4.2.2	Meshing size investigations	105

4.2.3 Effect of temperature ratio investigations	108
4.3 Computational investigation for diffused and compound cooling holes	113
4.3.1 Introduction	113
4.3.2 Results and discussion	113
4.4 Computational study of a new scheme for film-cooling hole (heart-shaped)	124
4.4.1 Introduction	124
4.4.2 Heart-shaped investigation results and discussion	124
4.5 Conjugate film cooling of a new multi-layers convex surface	138
4.5.1 Introduction	138
4.5.2 Multi-layers convex surface results and discussion	138
4.6 Conjugate film cooling of staggered configurations	148
4.6.1 Conjugate film cooling of two staggered rows	148
4.6.2 Conjugate film cooling of three staggered rows	154
4.7 Conjugate studies of the heart-shaped cooling holes	160
4.7.1 Heart-shaped coolant coverage on convex surface	160
4.7.2 Temperature distribution and heat flux on convex surface	164
4.7.3 Heart-shaped conjugate film cooling effectiveness	171

CHAPTER 5: CONCLUSION AND RECOMMENDATIONS

5.1 Conclusion	178
5.2 Recommendations	181
REFERENCES	182
LIST OF PUBLICATIONS	200
APPENDIX	201

LIST OF TABLES

Table 3.1: Geometrical parameters of the validation of three dimensional film cooling modeling.

Table 3.2: Physical parameters of the validation of three dimensional film cooling modeling.

Table 3.3: Geometrical and physical parameters of diffused and compound holes studies.

Table 3.4: Heart-shaped geometrical and physical parameters.

Table 3.5: Boundary conditions of conjugate multi-layers, conjugate one layer and adiabatic for A, B and C cases.

Table 3.6: Boundary conditions of conjugate staggered arrangement.

Table 3.7: Conjugate, heart-shaped, geometrical and physical parameters.

Table 3.8: The cooling hole geometries which have been used in this work of the thesis.

LIST OF FIGURES

Figure 1.1: Impingement cooling arrangement of a typical gas turbine airfoil (Han, et al.,2000).

Figure 1.2: Cooling concepts of a modern multi-pass turbine blade (Han, et al.,2000).

Figure 1.3: Sketch of film cooling technique.

Figure 1.4: A typical cooled airfoil (Han, et al.,2000).

Figure1.5: Sketch of film cooling technique on convex surface.

Figure 1.6: Flow structure of streamwise injection film cooling (Laboratory for Energy Conversion).

Figure 1.7: A flowchart encapsulating the various flow physics in CFD (Tu, et al., 2008).

Figure 1.8: Three-dimensional film cooling simulation (www.eng.fsu.edu).

Figure 2.1: Overview of hole geometries and coordinate system (Kim and Kim, 2004).

Figure 2.2: Experimental data comparison between the CYL, FANA and FANT for $M = 0.75$ (Bernier et al., 2009).

Figure 2.3: Experimental data comparison between the CYL, FANA and FANT for $M = 1.5$ (Bernier et al., 2009).

Figure 2.4: Louver film hole geometry (Ghorab et al., 2011).

Figure 2.5: Computational domain (Lee and Kim 2011).

Figure 2.6: Geometrical parameters (Lee and Kim 2011).

Figure 2.7: Definition of geometrical parameters (Heneka et al., 2012).

Figure 2.8: Geometries of three film cooling holes (Guangchao et al., 2008).

Figure 2.9: Top view of the continuous and discrete partial slot configurations (Black et al., 2011).

Figure 2.10: Details of film hole configurations (units in centimeters) (Wright et al., 2011).

Figure 2.11: Schematic of experimental setup (Yang and Zhang, 2012).

Figure 2.12: Schematic of the test model (Chen et al., 2011).

Figure 2.13: Film cooling test plate for $X/D = 6$, $Y/D = 5$ and hole angle 20 deg. (a) Test section dimensions and layout, where all dimensions are given in millimeters. (b) Test section coordinate system (Ligrani et al., 2012).

Figure 2.14: Shape hole geometry and test section (Yu et al., 2002).

Figure 2.15: Schematics of the selected film hole shapes, (a) cylindrical hole, (b) trenched cylindrical hole, (c) shaped hole and (d) trenched shaped hole (Baheri et al., 2008).

Figure 2.16: Sketch of the console configuration (Azzi and Jubran, 2007).

Figure 2.17 Computational grid around the hole for the computational model of the waist-shaped slot hole (Liu et al., 2012).

Figure 2.18: Hybrid film hole geometry (Ghorab and Hassan, 2010).

Figure 2.19: Geometry of the selected film cooling hole (Dai and Lin, 2011).

Figure 2.20: (a) cylindrical-shaped and (b) conical-shaped hole (Nguyen et al., 2011).

Figure 2.21: Schematic of (a) experimental set-up and (b) test section and coordinate system (Lee^b et al., 2002).

Figure 2.22: Schematic of the leading edge with 4D hole spacing (Mehendale and Han, 1992).

Figure 2.23: Configuration of the test model (Liu et al., 2012).

Figure 2.24: Configuration of the film holes (Liu et al., 2012).

Figure 2.25: Curved wall film cooling test facility (Lutum et al., 2000).

Figure 2.26: Convex test section with constant converging channel (Lutum^b et al.,2001)

Figure 2.27: Schematic view of test facility (Lee et al., 2005).

Figure 2.28: The geometry, (a) test pieces, (b) two rows of circular straight holes, (c) two rows of forward-expanded holes (Lee et al., 2005).

Figure 2.29: Seven-row film cooling leading edge models, (a) radial angle cylindrical holes, (b) compound angle cylindrical holes, (c) radial angle shaped holes and (d) compound angle shaped holes (Gao and Han, 2009).

Figure 2.30: Three-row film cooling leading edge models, (a) radial angle cylindrical holes, (b) compound angle cylindrical holes, (c) radial angle shaped holes and (d) compound angle shaped holes (Gao and Han, 2009).

Figure 2.31: Schematic of test section (Lee^c et al., 2002).

Figure 2.32: Leading edge model (Takahashi et al., 2012).

Figure 2.33: Nusselt number contours for (a) $Re_j = 20,000$; (b) $Re_j = 28,000$; (c) $Re_j = 40,000$ at blowing ratio of 1.4 (Wang et al., 2011).

Figure 3.1: Computational domain showing boundary conditions.

Figure 3.2: Step S1a, plenum and two cylinders are one volume and have meshed with relatively fine tetrahedral.

Figure 3.3: Step S1b, plenum and the two cylinders are connected by two interfaces and have meshed with relatively fine hexahedral.

Figure 3.4: Three different cases of film cooling holes, (a) case A: simple cylinder, (b) case B: diffused and (c) case C: compound, besides, three types of arrangements, one row, two staggered rows and three staggered rows.

Figure 3.5: Three dimensional model for three staggered rows of diffused hole.

Figure 3.6: Three film cooling holes, (a) simple cylinder cooling hole, (b) diffused cooling hole, and (c) compound cooling hole.

Figure 3.7: Three-dimensional sketch for the (a) heart-shaped cooling hole and the (b) computational model.

Figure 3.8: Comparative sketch between the (a) simple cylinder hole and the (b) heart-shaped hole, illustrating vortex mitigation in the heart-shaped hole.

Figure 3.9: (a) Computational domain of multi-layers state, (b) three different film cooling hole cases.

Figure 3.10: Sketch for multi-layers showing heat absorption process from the convex surface.

Figure 3.11: Three different cases of cooling holes and staggered arrangements.

Figure 3.12: heart-shaped cooling hole.

Figure 3.13: Three different cooling holes arrangements.

Figure 3.14: Conjugate heart-shaped, computational domain and boundary conditions.

Figure 4.1: Centerline ($Z/3D=0$) adiabatic film cooling effectiveness study for step S1, meshing type investigation.

Figure 4.2: Centerline ($Z/3D=0$) adiabatic film cooling effectiveness study for step S2, meshing size investigation of the plenum and cylinders.

Figure 4.3: Lateral ($Z/3D=0.5$) adiabatic film cooling effectiveness study for step S2, meshing size investigation of the plenum and cylinders.

Figure 4.4: Centerline ($Z/3D=0$) adiabatic film cooling effectiveness study for step S3, the various values of temperature ratio, T_c/T_g investigation.

Figure 4.5: Lateral ($Z/3D=0.5$) adiabatic film cooling effectiveness study for step S3, the various values of temperature ratio, T_c/T_g investigation.

Figure 4.6: Total temperature (K) contour on the convex surface with isosurfaces showing the film cooling development for $T_c/T_g=0.6$.

Figure 4.7: The flow downstream at specified axial distance, X/D for four temperature ratios investigated.

Figure 4.8: (a) visualization of temperature contour, (b) centerline and lateral adiabatic film cooling effectiveness at $X/D = 5$, (c), iso-surface intersection visualization at $X/D=5$ for three hole cases, case A (simple cylinder hole), case B (diffused hole) and case C (compound hole).

Figure 4.9: Comparison of centerline and lateral adiabatic film cooling effectiveness at $X/D=5$ for three kinds of holes, case A (simple cylinder hole), case B (diffused hole) and case C (compound hole).

Figure 4.10: Centerline ($Z/3D=0$) adiabatic film cooling effectiveness for one row of three kinds of holes, case A (simple cylinder hole), case B (diffused hole) and case C (compound hole) were compared with the experimental data.

Figure 4.11: Lateral ($Z/3D=0.5$) adiabatic film cooling effectiveness for one row of three kinds of holes, simple hole, diffused hole and compound hole were compared with the experimental data.

Figure 4.12: Centerline ($Z/3D=0$) adiabatic film cooling effectiveness for two staggered rows of three kinds of holes, simple hole, diffused hole and compound hole.

Figure 4.13: Contour of total temperature for two staggered rows of three kinds of holes, simple hole, diffused hole and compound hole.

Figure 4.14: Centerline ($Z/3D=0$) adiabatic film cooling effectiveness for three staggered rows of three kinds of holes, simple hole, diffused hole and compound hole.

Figure 4.15: Total temperature contour for three staggered rows of three kinds of cooling holes, simple hole, diffused hole and compound hole.

Figure 4.16: Comparison for Centerline ($Z/3D=0$) adiabatic film cooling effectiveness for the three cases, A, B and C for one row, two staggered rows and three staggered rows, besides the experimental data.

Figure 4.17: Results of the investigation of the vortexes in the three cooling hole cases (A, D and E) on a surface perpendicular to the axis of the flow at $X/D = 5$.

Figure 4.18: Centerline and lateral adiabatic film cooling effectiveness at $X/D = 5$ for the three cases of cooling holes: case A with simple hole, case D with heart-shaped hole ($\varphi = 60^\circ$), and case E with heart-shaped hole ($\varphi = 90^\circ$).

Figure 4.19: Comparison of centerline and lateral adiabatic film cooling effectiveness at $X/D = 5$ for the three cases of cooling holes, A, D and E.

Figure 4.20: Centerline ($Z/3D = 0$) adiabatic film cooling effectiveness for one row of Case A, Case D, and Case E, with experimental data.

Figure 4.21: Contour of total temperature of one row, two staggered rows, and three staggered rows for case D and case E.

Figure 4.22: Lateral ($Z/3D = 0.5$) adiabatic film cooling effectiveness for one row of case A, case D, and case E, with experimental data.

Figure 4.23: Centerline ($Z/3D = 0$) adiabatic film cooling effectiveness for two staggered rows of case A, case D, and case E.

Figure 4.24: Centerline ($Z/3D = 0$) adiabatic film cooling effectiveness for three staggered rows of case A, case D, and case E.

Figure 4.25: Comparison of centerline ($Z/3D = 0$) adiabatic film cooling effectiveness for different cases and arrangements of the heart-shaped, with experimental data.

Figure 4.26: Temperature contour for three staggered rows of case D (heart-shaped $\phi = 60^\circ$), showing the film cooling development over the convex surface.

Figure 4.27: Methane tracer on the convex surface of case B.

Figure 4.28: Contour of total temperature for adiabatic, one layer conjugate and multi-layers conjugate for three different hole cases.

Figure 4.29: Contour of surface Nusselt number for multi-layers conjugate and one layer conjugate for three different hole cases.

Figure 4.30: Contour of total heat flux for multi-layers conjugate and one layer conjugate for three different hole cases.

Figure 4.31: Centerline ($Z/3D = 0$) film cooling effectiveness for all the states of the three cases, A, B and C.

Figure 4.32: Lateral ($Z/3D = 0.5$) film cooling effectiveness for all the states of the three cases, A, B and C.

Figure 4.33: Methane tracer on convex surface for two staggered rows of case B.

Figure 4.34: Temperature contour of adiabatic and conjugate film cooling of two staggered rows of cases, A, B and C.

Figure 4.35: Conjugate and adiabatic centerline ($Z/3D = 0$) film cooling effectiveness for two staggered rows of cases, A, B and C.

Figure 4.36: Contour of surface Nusselt number for the conjugate of two staggered rows, case A, case B and case C.

Figure 4.37: Contour of total surface heat flux for the conjugate of two staggered rows, case A, case B, and case C.

Figure 4.38: Methane tracer on convex surface for three staggered rows of case B.

Figure 4.39: Temperature contour of adiabatic and conjugate film cooling of three staggered rows for (a) case A, (b) case B and (c) case C.

Figure 4.40: Contour of surface Nusselt number for the conjugate of three staggered rows for (a) case A, (b) case B and (c) case C.

Figure 4.41: Contour of total surface heat flux for the conjugate of three staggered rows for (a) case A, (b) case B and (c) case C.

Figure 4.42: Conjugate and adiabatic centerline ($Z/3D=0$) film cooling effectiveness for three staggered rows of cases, A, B and C.

Figure 4.43: Methane tracer on convex surface for different configurations of heart-shaped, case D.

Figure 4.44: Methane tracer on convex surface for different configurations of heart-shaped, case E.

Figure 4.45: Methane tracer on convex surface for different configurations of simple cylinder, case A.

Figure 4.46: Contour of (a) total temperature, (b) surface Nusselt number and (c) total surface heat flux, one row, case D.

Figure 4.47: Contour of (a) total temperature, (b) surface Nusselt number and (c) total surface heat flux, two rows, case D.

Figure 4.48: Contour of (a) total temperature, (b) surface Nusselt number and (c) total surface heat flux, three rows, case D.

Figure 4.49: Contour of (a) total temperature, (b) surface Nusselt number and (c) total surface heat flux, one row, case E.

Figure 4.50: Contour of (a) total temperature, (b) surface Nusselt number and (c) total surface heat flux, two rows, case E.

Figure 4.51: Contour of (a) total temperature, (b) surface Nusselt number and (c) total surface heat flux, three rows, case E.

Figure 4.52: Centerline conjugate and adiabatic film cooling effectiveness, one row, case D.

Figure 4.53: Centerline conjugate and adiabatic film cooling effectiveness, one row, case E.

Figure 4.54: Conjugate and adiabatic lateral film cooling effectiveness, one row, case D, case E and baseline.

Figure 4.55: Centerline conjugate and adiabatic film cooling effectiveness, two staggered rows, case D.

Figure 4.56: Centerline conjugate and adiabatic film cooling effectiveness, two staggered rows, case E.

Figure 4.57: Centerline conjugate and adiabatic film cooling effectiveness, three staggered rows, case D.

Figure 4.58: Centerline conjugate and adiabatic film cooling effectiveness, three staggered rows, case E.

Figure 4.59: Centerline conjugate and adiabatic film cooling effectiveness of different configurations and cases of the heart-shaped.

LIST OF SYMBOLS

C_2 and $C_{1\epsilon}$	Constants.
D	Injection hole diameter (cm).
D_h	Hydraulic diameter (m).
G_b	The generation of turbulence kinetic energy due to buoyancy.
G_k	The generation of turbulence kinetic energy due to the mean velocity gradient.
h	Heat transfer coefficient ($\text{W}/\text{m}^2\text{K}$).
h_{af}	Adiabatic film heat transfer coefficient, $h_{af} = q''/(T_{aw}-T_w)$ ($\text{W}/\text{m}^2\text{K}$).
\vec{J}_j	The diffusion flux of species j .
K	Thermal conductivity in solid regions ($\text{W}/\text{m K}$).
κ	Turbulent kinetic energy.
k_f	Thermal conductivity of air ($\text{W}/\text{m K}$).
k_{eff}	The effective conductivity.
M	Blowing ratio.
N_u	Nusselt number.
Pr	Prandtl number.
p	Static pressure (N/m^2).

q''	Heat flux (W/m ²).
q''/q_0''	Heat flux ratio.
r	Radius of curvature of convex surface (cm).
Re_c	Coolant Reynolds number.
Re_g	Main hot gas Reynolds number.
S_h	Includes the heat of chemical reaction and any other volumetric heat sources that could be defined.
S_k and S_ϵ	User defined source terms.
$T_{aw,con.}$	Adiabatic wall temperature(for adiabatic case) or conjugate wall temperature (for conjugate case) (K).
T_c	Coolant temperature (K).
T_g	Main hot gas temperature (K).
T_w	Wall surface temperature in contact with gas (K).
Tu	Turbulence Intensity (%).
u_j	Cartesian velocity component.
u^*	Friction velocity; $u^* = (\tau_w / \rho)^{1/2}$ (m/s).
V_c	Coolant velocity (m/s).
V_g	Main hot gas velocity (m/s).

- y^+ The normalized distance; $y^+ = yu^*/\nu$.
- y Coordinate normal to the test surface (m).
- Y_M The contribution of the fluctuating dilatation in compressible turbulence to the overall dissipation rate.

Greek letters

- α Cooling hole inclination angle (deg).
- β Diffused angle (deg).
- $\eta_{aw,con.}$ Adiabatic film cooling effectiveness (for adiabatic case) or conjugate film cooling effectiveness (for conjugate case), $\eta_{aw,con.} = \frac{T_g - T_{aw,con.}}{T_g - T_c}$.
- μ Molecular viscosity (Ns/m²).
- μ_t Turbulent viscosity.
- σ_κ and σ_ϵ Turbulent Prandtl number for κ and ϵ respectively.
- ρ Density of the air (Kg /m³).
- φ Crown's angle of heat-shaped film cooling hole (deg).
- Φ Film cooling effectiveness, $\Phi = (T_g - T_w)/(T_g - T_c)$, $\Phi_o = (T_g - T_{wo})/(T_g - T_c)$.
- τ_w Wall shear stress (N/m²).
- ν Kinematic viscosity (m²/s).

Subscripts

aw Adiabatic wall.

c Coolant flow.

con. Conjugate.

g Main hot gas.

f Fluid.

w Wall.

f and *o* With and without film cooling respectively.

KAJIAN BERANGKA BAGI KESAN PARAMETER GEOMETRI KE ATAS PRESTASI PENYEJUKAN FILEM

ABSTRAK

Tujuan kajian ini adalah untuk mengkaji kesan pelbagai jenis lubang penyejukan dan susunan secara stagak ke atas keberkesanan penyejuk filem adiabatik dan konjugat bagi permukaan melengkung bagi bilah turbin gas. Kajian termaksud skim lubang baru yang dikenali bentuk jantung untuk menyelesaikan masalah vortex yang menyebabkan fenomena merugikan vorteks terangkat bagi lubang penyejukan filem silinder mudah konvensional.

Juga, kajian konjugat termaksud sebuah teknik bilah konjugat baru yang dipanggil pelbagai lapisan dapat membantu bagi mencepatkan penyerapan haba daripada permukaan bilah atas. FLUENT telah digunakan dan model “Realizable k- ϵ ” digunakan. Selain itu, persamaan tenaga telah diselesaikan. Kajian tak bergantung jaringan telah disempurnakan. Kajian nisbah suhu diantara penyejuk dan gas panas aliran utama T_c/T_g telah dijalankan dengan menggunakan empat nilai nisbah, iaitu, 0.5, 0.6, 0.7 dan 0.8. Nisbah suhu $T_c/T_g = 0.6$ mendapati persetujuan baik dengan data eksperimen bagi semua model lain dan model telah ditentukan. Pengesahan ini memberikan garis aras bagi kajian seterusnya dalam pengoptimuman bagi menentukan keberkesanan filem.

Kajian optimum bagi keberkesanan penyejukan filem adiabatik dijalankan bagi susunan siri dan stagak untuk baris dua dan tiga. Sebuah lubang 10° tercapah ($\beta = 10^\circ, \gamma = 0^\circ$) dan lubang gabungan 10° dan 45° tercapah pada arah arus aliran hilir ($\beta = 10^\circ, \gamma = 45^\circ$) lubang penyejukan filem telah dikaji dan dibandingkan dengan penyejukan filem lubang mudah ($\beta = 0^\circ, \gamma = 0^\circ$) dipermukaan melengkung.

Kajian bagi sebuah skim noval yang dipanggil lubang penyejukan filem berbentuk jantung telah dijalankan. Kajian komputer tiga dimensi bagi sebaris, baris dua stagak, dan baris tiga stagak dijalankan pada sebuah permukaan melengkung. Dua lubang berbentuk jantung dengan kedua-dua sudut mahkota, $\phi = 60^\circ$ dan $\phi = 90^\circ$ dijalankan bagi menentukan keberkesanan penyejukan filem adiabatik.

Pemindahan haba konjugat dan kajian keberkesanan penyejukan filem disepanjang permukaan melengkung bagi lubang penyejukan satu baris, baris dua stagak dan baris tiga stagak telah dijalankan. Lubang silinder mudah, lubang tercapah, lubang gabungan dan lubang berbentuk jantung juga dijalankan. Keluli tahan karat digunakan sebagai bahan padu bagi kes konjugat. Methan tak boleh bakar 10000p.p.m. digunakan sebagai gas pengesan didalam campuran penyejuk. Teknik permukaan melengkung pelbagai lapisan bagi keluli tahan karat-aluminium-keluli tahan karat dikaji dan dibandingkan dengan kes konjugat satu lapisan keluli tahan karat dan adiabatik.

Keputusan menunjukkan lubang berbentuk jantung memberikan peningkatan ketara keberkesanan penyejukan filem adiabatik di garis pusat dan sisi bagi kedua-dua sudut mahkota, $\phi = 60^\circ$ dan $\phi = 90^\circ$. Isipadu kecil secara relatif dan keberkesanan tinggi bagi lubang penyejukan berbentuk jantung adalah penting dan menyakinkan untuk industri enjin aero. Agihan lubang stagak tercapah dan gabungan memberikan perlindungan yang tinggi untuk permukaan melengkung berbanding lubang silinder mudah. Perbezaan ketara dalam agihan suhu di atas permukaan telah ditunjukkan diantara kes konjugat dan adiabatik. Aras suhu permukaan melengkung bagi teknik pelbagai lapisan adalah rendah daripada konjugat satu lapisan dan adiabatik. Seperti yang dijangkakan teknik baru ini boleh diganding bersama dalam pembangunan turbin gas moden.

NUMERICAL INVESTIGATION ON THE EFFECTS OF GEOMETRICAL PARAMETERS ON FILM COOLING PERFORMANCE

ABSTRACT

The aim of this study is to investigate the effect of different kinds of cooling holes and staggered arrangements on adiabatic and conjugate film cooling effectiveness for convex surface of gas turbine blade. The investigation included a new cooling hole scheme called heart-shaped to solve the vortex problem claimed to be responsible for the detrimental lift-off phenomenon in conventional simple cylinder film cooling holes.

Also, the conjugate studies included a new conjugate blade technique called multi-layers to be helpful in speeding up the heat absorption from the upper blade surface. Fluent[®] has been utilized and realizable κ - ϵ turbulent model has been used. Besides, the energy equation has been solved. Grid independence study has been fulfilled. Study of temperature ratio between the coolant and the mainstream hot gas T_c/T_g has been performed using four values of temperature ratios, namely, 0.5, 0.6, 0.7, and 0.8. Temperature ratio of $T_c/T_g = 0.6$ found to be in good agreement with the experimental data among all of the other models and the model has been validated. This computational validation serves as the baseline for further studies of optimization in determining the film cooling effectiveness.

Optimization studies for adiabatic film cooling effectiveness have been conducted for in-lined and staggered arrangements of two and three rows. A 10° diffused hole ($\beta = 10^\circ$, $\gamma = 0^\circ$) and compound hole of 10° diffused and 45° with the downstream direction ($\beta = 10^\circ$, $\gamma = 45^\circ$) film cooling holes have been investigated and have been compared with that of simple hole ($\beta = 0^\circ$, $\gamma = 0^\circ$) film cooling on convex surface.

Investigation for a novel scheme called heart-shaped film cooling hole is performed. Three-dimensional computational study for one row, two staggered rows, and three staggered rows have been conducted on a convex surface. Two heart-shaped holes of two crown angles, $\varphi = 60^\circ$ and $\varphi = 90^\circ$, are conducted to ascertain adiabatic film cooling effectiveness.

Conjugate heat transfer and film cooling effectiveness studies along the convex surface for one cooling hole row, two staggered rows and three staggered rows were performed. Simple cylinder hole, diffused hole, compound hole and heart-shaped holes were investigated. Stainless steel was used as the solid material in the conjugate case. Non-combustible methane of 10000p.p.m. was used as the tracer gas in the coolant mixture. Multi-layers convex surface technique of stainless steel-aluminum-stainless steel was investigated and compared with conjugate of one layer of stainless steel and adiabatic case.

The results indicated that the heart-shaped provides a tremendous increment in centerline and lateral adiabatic film cooling effectiveness for both crown angles, $\varphi = 60^\circ$ and $\varphi = 90^\circ$. The relatively small volume and high effectiveness of the heart-shaped cooling hole is important and promising for the aero engine industry. The staggered distribution of diffused and compound holes provides higher protection for the convex surface compared to the simple cylinder hole. Significant difference in the temperature distributions on the convex surface have been shown between the conjugate cases and adiabatic cases. The temperature level of convex surface in multi-layers technique is lower than the one layer conjugate and adiabatic. Expectedly this new technique will be cooperative in developing the modern gas turbine.

CHAPTER 1

INTRODUCTION

1.1 Film Cooling

Modern gas turbine engines play an important role in aeronautical propulsion and future power generation systems. Modern gas turbine engines are designed to perform at high inlet temperature of approximately 1800-2000K. Any increase in the thermal efficiency of a gas turbine engine is contingent on corresponding increases of the turbine inlet temperature.

In order for the blade to withstand such adverse environment and avoid any material failure it becomes essential to provide an arrangement for cooling system to ensure that the maximum blade surface temperature during operation is not more than the maximum melting point of the blade material. It should be noted that an under-prediction of the blade surface temperature of only 15K may reduce the life time up to 50%. Thus turbine inlet temperature cannot be increased further without effective cooling technique to protect turbine materials from melting down.

Of the various cooling mechanisms available, film cooling has come to be widely accepted as one of the more useful and active cooling method. Depending on the nature of the coolant flow, the cooling methods currently implemented in the turbine industry can be classified into two types, internal cooling and external cooling. In the internal cooling the coolant air is bled from the compressor stage and then passed through internal passages incorporated in to blade designs for this purpose. Figure 1.1 illustrated jet impingement configuration in the midchord region for a typical gas turbine airfoil.

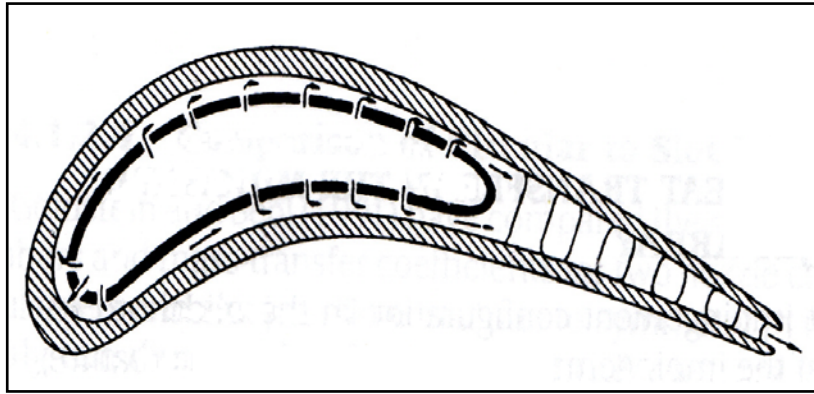


Figure 1.1: Impingement cooling arrangement of a typical gas turbine airfoil (Han, et al., 2000).

For the external cooling, the air is bled from the compressor stage, ducted through the internal chambers of the turbine blades, and then discharged through small holes/ slots onto the blade outer walls as shown in Figure 1.2.

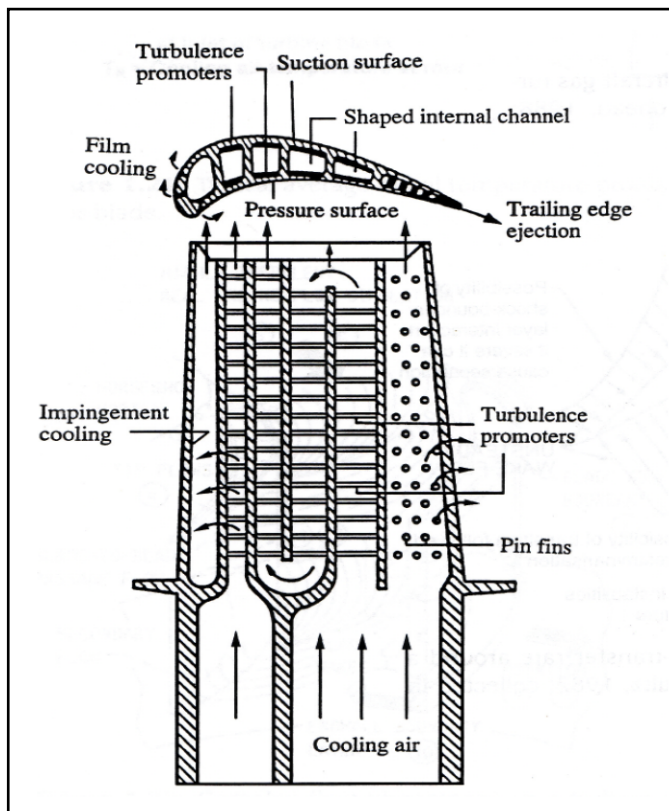


Figure 1.2: Cooling concepts of a modern multi-pass turbine blade (Han, et al., 2000).

The air provides a thin, cooler, insulating film along the external surface of the turbine blade, due to which the method is called film cooling as shown in Figure 1.3.

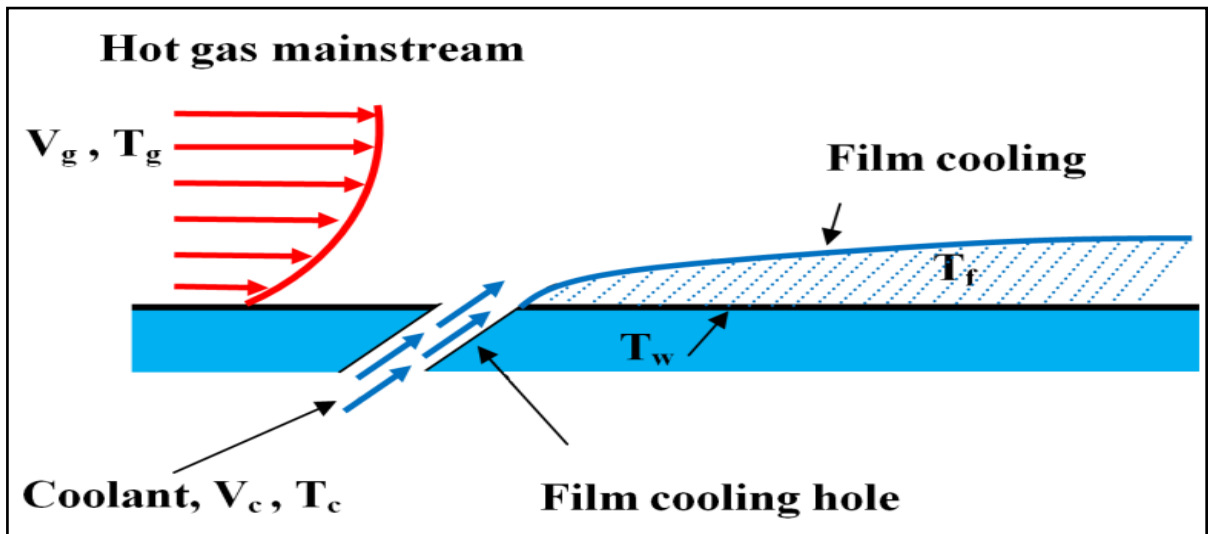


Figure 1.3: Sketch of film cooling technique.

This film provides a thin protection layer to the adjacent wall of components in the gas turbine engine thus increases the life of the components and reduce the maintenance requirements (Han, et al., 2000). The film cooling technique is applicable to turbine blade as illustrated in Figure 1.4.

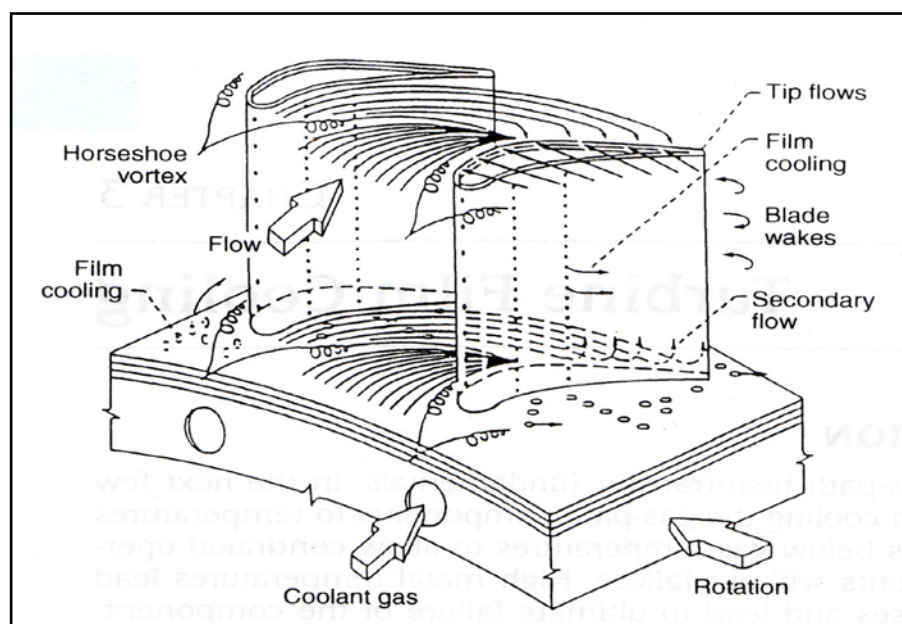


Figure 1.4: A typical cooled airfoil (Han, et al., 2000).

Film cooling depends primarily on many physical and geometrical parameters which include pressure ratio, temperature ratio, blowing ratio, and the shape of the film cooling hole. In addition, the distribution of these cooling holes on the airfoil and the inclination angles also are at paramount aspect into consideration. In a typical gas turbine, the blowing ratio varies from 0.5 to 2.0 whereas temperature ratio varies from 0.5 to 0.85. Since the temperature ratio essentially provides the ratio of the coolant to hot mainstream thermal capacitance, it is useful measure in quantifying film cooling effectiveness. Consequently will be helpful to know where the heat is transferred from the hot gas mainstream to the airfoil, thus it will be helpful in designing a good film cooling pattern for better film cooling performance.

As a complex interaction between the mainstream and the coolant, the film cooling performance is known to be affected by the gas turbine airfoil curvature. The pressure surface (concave surface) or suction surface (convex surface) is very important in film cooling studies. The pressure gradients due to the curvature, affects the film cooling effectiveness compared to a flat surface. Figure 1.5 shows sketch for film cooling over a convex surface.

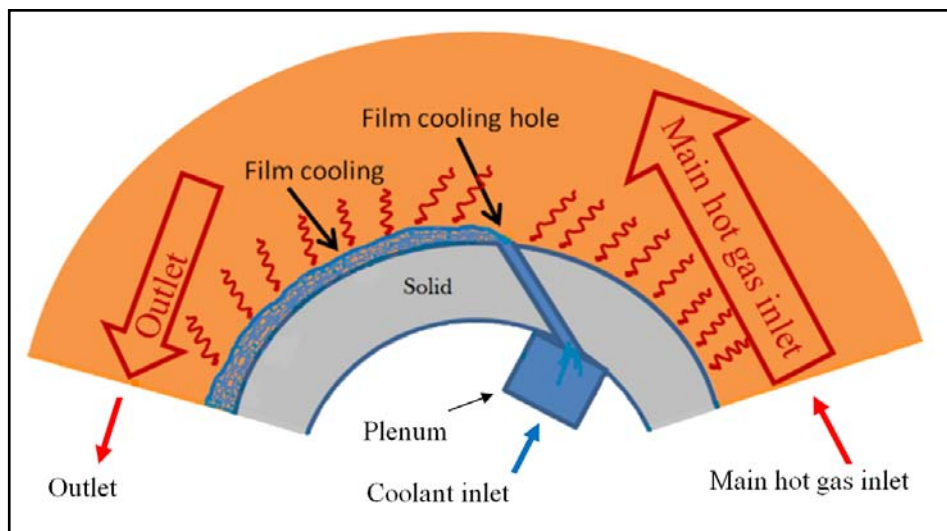


Figure 1.5: Sketch of film cooling technique on convex surface.

1.2 Film cooling fundamentals

In film cooling technique, coolant jet (usually air) is injected through discrete film cooling holes onto the surface of the blade, to provide a thin layer of cool air downstream of the film cooling hole which insulates the blade surface from the hot main stream and provide good protection to the blade from failure. Since the coolant jet which ejected into the holes is extracted from the compressor, poor management of the cooling air can be otherwise detrimental to the engine overall efficiency. Therefore the design of film cooling must be optimized to minimize the aerodynamic loss associated with film cooling. Figure 1.6 shows the flow structure of injection film cooling. The flow structure clearly illustrates the kidney vortices claimed to be responsible for lift-off phenomenon consequently it is detrimental to the film cooling performance.

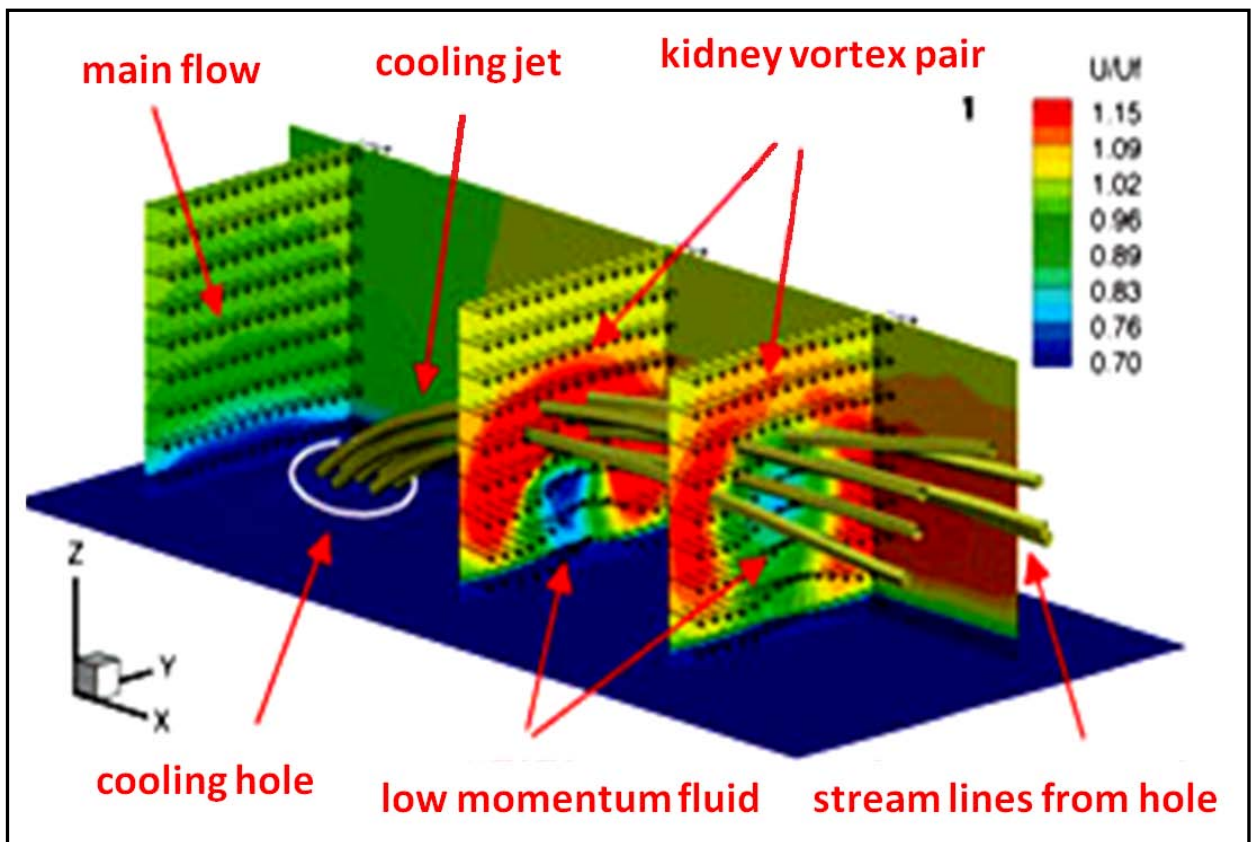


Figure 1.6: Flow structure of streamwise injection film cooling (Laboratory for Energy Conversion).

Heat flux is the rate of heat transfer through a given surface. The heat load to the surface without film cooling is represented as heat flux (q_o'') as given in equation 1:

$$q_o'' = h_o(T_g - T_w) \quad (1)$$

In equation 1, the heat flux highly depends on the difference between the gas temperature and the wall temperature. When coolant is injected on the surface, the film temperature T_f becomes the driving temperature, because it is near to the surface and then the heat load to the surface q is given as in equation 2:

$$q'' = h(T_f - T_w) \quad (2)$$

Once again in equation 2, the heat flux depends on the difference between two different temperatures, the film cooling temperature and the wall temperature. The heat flux ratio ($\frac{q''}{q_o''}$) can be written as in equation 3:

$$\frac{q''}{q_o''} = (h/h_o)[(T_f - T_w)/(T_g - T_w)] \quad (3)$$

In equation 3, the heat flux ratio, in addition to its dependence on the temperature differences ratio, the ratio of the heat transfer coefficient is of great concern.

Also an important term using film cooling effectiveness (η) is introduced as in equation 4:

$$\frac{q''}{q_o''} = \frac{h}{h_o} [1 - \eta \frac{T_g - T_c}{T_g - T_w}] \quad (4)$$

In equation 4, η is vital indicator to test film cooling performance. As film cooling experimental studies are usually conducted on an adiabatic plate so η in that case is called as adiabatic film cooling effectiveness or conjugate film cooling effectiveness for conjugate case.

The heat flux ratio (q''/q_o'') according to the recent study by (Wang and Zhao, 2011) defined as in equation 5:

$$\frac{q''}{q_o''} = \frac{h_{af}}{h_o} \left(1 - \frac{\eta}{\Phi_o}\right) + \frac{h_{af}}{h_o} \cdot \frac{\Phi - \Phi_o}{\Phi_o} \quad (5)$$

1.2.1 Film cooling effectiveness

The performance of the film cooling is expressed mathematically by film cooling effectiveness defined in equation 6.

$$\eta_{aw,con.} = \frac{T_g - T_{aw,con.}}{T_g - T_c} \quad (6)$$

The values of η vary between 1 which represent perfect film cooling and 0 which represent no film cooling. It is necessary to understand the physics of film cooling flows and their effect on film cooling effectiveness. The best film cooling design is to reduce the heat load ratio with greater η for minimum amount of coolant available for a film cooled airfoil. Hence, film cooling technique is still in the process of both improvement and optimization for better film cooling effectiveness.

1.2.2 Conjugate film cooling

The conduction through the wall strongly affects the temperature distribution on the blade surface. In this situation, in addition to the big number of physical and geometrical parameters that influence the performance of the film cooling technique in an adiabatic case, there would be an additional important process, which is the heat transfer into the solid bulk of the blade. Therefore, if a realistic prediction of the solid surface temperature sought, a solution of the convection and conduction is necessary. Coupling the heat transfer in the fluid with the heat conduction inside the solid surface is termed as conjugate heat transfer. In conjugate film cooling, the heat transfer problem is three-dimensional problem, along the wall in addition to the conduction from outer to inner

wall. Besides, the film cooling is a two-temperature problem, which causes the direction of heat flux at the wall to change over the outer surface, from the wall into the fluid at some positions and reverse its direction to the wall at other positions. The heat transfer coefficient is frequently defined in term of Nusselt number Nu , as in equation 7. In heat transfer at a surface within a fluid, the Nusselt number (Nu) is the ratio of convective to conductive heat transfer.

$$N_u = hD_h/k_f \quad (7)$$

Also the heat transfer coefficient can be defined as in equation 8:

$$h = \frac{q_w}{T_w - T_f} \quad (8)$$

Hence, equation 7 can be rewritten as in equation 9:

$$N_u = \frac{q_w D_h}{k_f (T_w - T_f)} \quad (9)$$

For a fully developed channel flow, Nusselt number is frequently given in term of Reynolds number and prandtl number as in Dittus-Boelter correlation given in equation 10.

$$N_u = 0.023 Re^{0.8} Pr^{0.4} \quad (10)$$

1.2.3 Computational fluid dynamic (CFD) for effectiveness prediction

The experimental heat transfer covers approximately half century of research, during which developed significant new designs to increase the efficiency of turbine components that are subject to harsh operating temperature. Although the designers expected to gather actual information and data for heat transfer under real experimental

turbine condition, it is very difficult to obtain results under real engine condition experiment. Thus there is lack in the experiments of real engine conditions.

Computational fluid dynamic provide the superior alternative to obtain the details that are impossible to obtain by experimental means. CFD thus far does not suggest that it will soon replace experimental testing. Instead it is considered a viable alternative (Tu, et al., 2008) The experimental data are often used to validate the computational solutions (Graf, Kleiser, 2011).

The computational analysis is then utilized to shorten the design cycle by controlling the parametric studies, consequently reducing the required amount of experimental testing. Nowadays the simulations for film cooling investigation getting more important due to its low-cost, labor-saved and complete-data characteristics (Liu, et al., 2011).

In modern film cooling studies, CFD can be used to capture flow and heat transfer details accurately and provide logic for determining the reasons for increasing or decreasing in film cooling performance (Hyams, Lylek, 2000). In addition the increase in the computer powers has made it economical to optimize the design parameters based on computational analysis. Figure1.7 presents the various flow physics that may be encountered within the framework of CFD and heat transfer processes (Tu, et al., 2008).

In real gas turbines, sharp edges are an approximation because of manufacturing geometrical modifications occurring during operation. Consequently leads to an impact in film cooling configuration. Fortunately, manufacturing uncertainty can be predicted by CFD (Montomoli, et al., 2012). Also, using CFD, the researchers are able to estimate the penalty for turbine efficiency associated with film cooling for a turbine stage (Lim, et al., 2012).

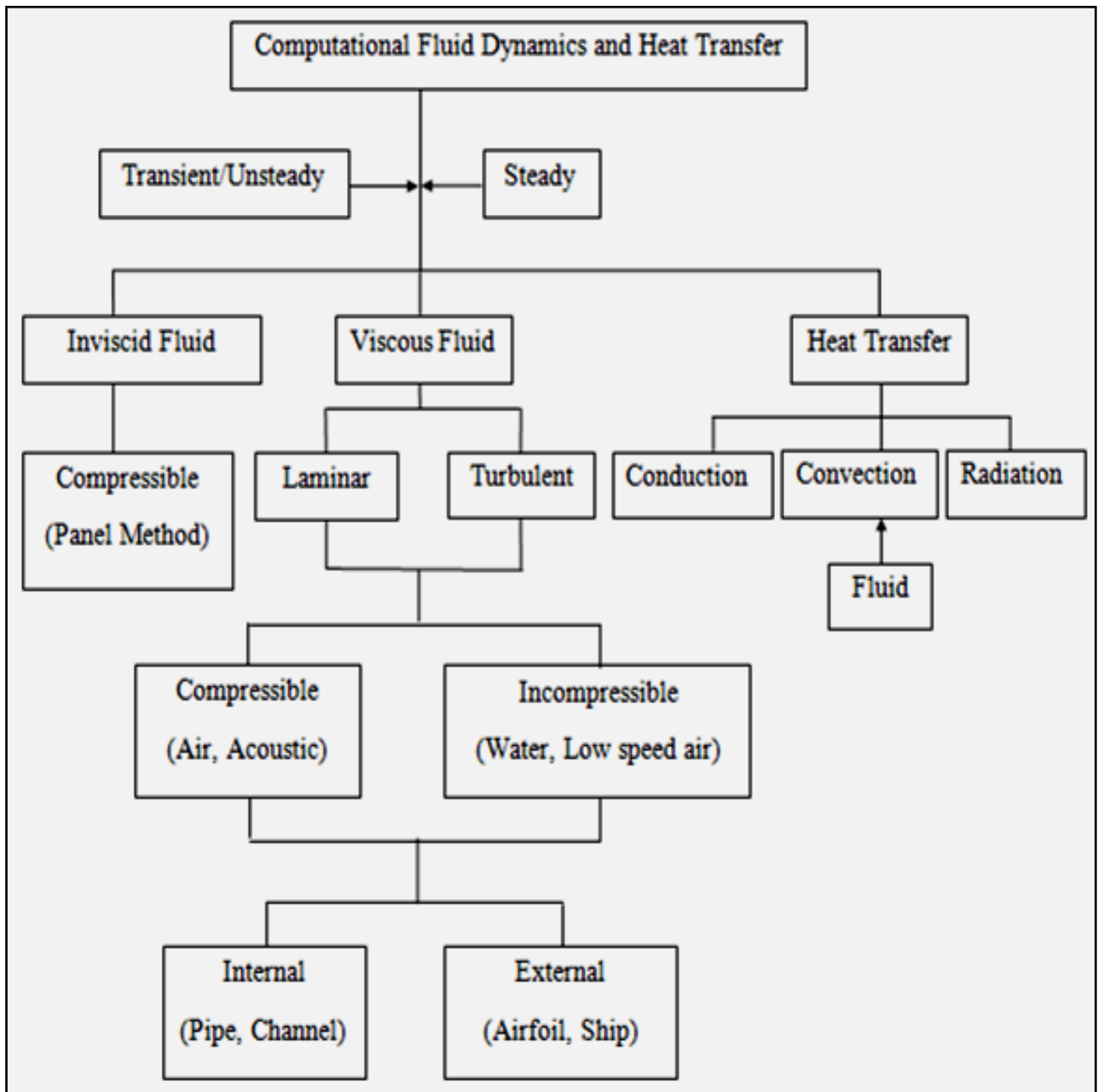


Figure 1.7: A flowchart encapsulating the various flow physics in CFD (Tu, et al., 2008).

The turbulent models which developed by some researchers improved the quality of the numerical production significantly. In addition computational fluid dynamic provides clear visualization as shown in Figure 1.8. Most external heat transfer predictions are done with time-averaged turbulence models such as κ - ϵ turbulence model. Hence throughout this dissertation FLUENT[®] software has been used and realizable κ - ϵ was used as a turbulence model.

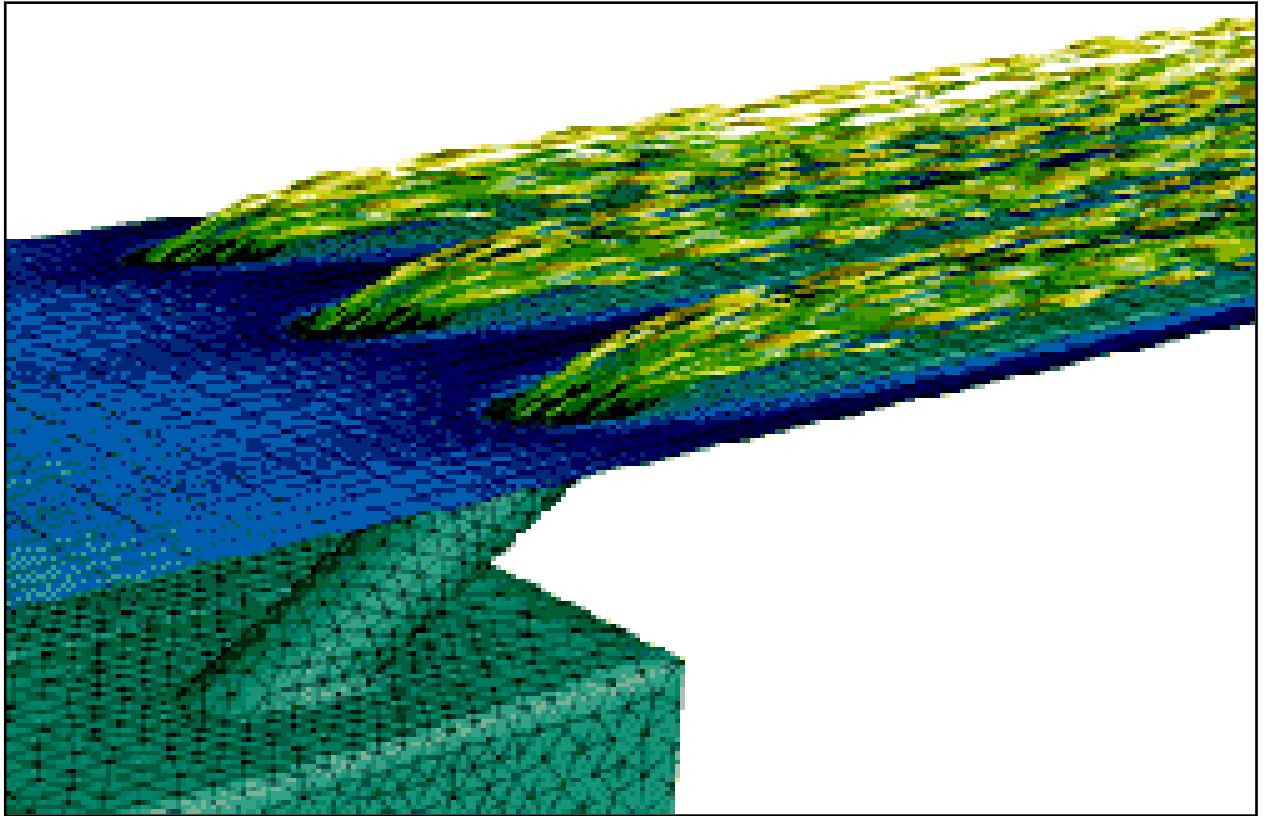


Figure 1.8: Three-dimensional film cooling simulation (www.eng.fsu.edu).

1.3 Problem Statement

Gas turbine engines are becoming the choice for current and future power generation system. Modern gas turbine engines are designed to perform at high inlet temperature of approximately 2000K. Unfortunately these higher temperatures have a negative effect on the integrity of the high pressure turbine components and specifically the turbine blade.

Although the strength of alloys at high temperature has improved, a gas turbine provides a temperature and stress environment which is beyond the limit alloys can presently achieve without cooling.

At the same time, less cooling air will be available as more of the air will be used for combustion. Thus, improved cooling technique is requiring minimum usage of air.

Film cooling technique is still an effective cooling technique. The film cooling performance is known to be affected by variety of parameters such as the blade surface curvature, hole arrangement and configuration, injection angle, blowing ratio, Reynolds number of the mainstream and the coolant, momentum ratio etc.

The interaction between the hot mainstream and the injected coolant can drastically alter the flow condition, in turn causing the magnitude of the effectiveness to be changed according to the nature of the interaction. The shape and configurations of the film cooling holes have vital influence on the film cooling effectiveness.

1.4 Objectives

- To investigate different kinds of film cooling holes for adiabatic and conjugate film cooling effectiveness on convex surface of hot gas turbine components.
- To investigate a new cooling hole scheme called heart-shaped to mitigate the lift-off phenomenon of conventional cooling holes.
- To investigate a new conjugate blade technique called multi-layers to be helpful in speeding up the heat absorption from the upper blade surface.
- To make recommendations based on the heat transfer and film cooling effectiveness enhancement, cooling hole design and cooling hole configuration.

1.5 Scope of the work

The scope of this study includes computational fluid dynamic investigations of different kinds of film cooling holes on convex surface using FLUENT[®]. The adiabatic and conjugate film cooling effectiveness have been considered.

The film cooling is opted due to it is unique and efficient way to protect the turbine blade from the high temperature exposure. Film cooling is an external cooling technique in which a coolant is ejected through discrete holes over the surface of the components that need thermal protection. The stages, in general, involved in this work are given as follow:

- Three dimensional Computational fluid dynamic for validation an experimental data of the literature to be baseline for further film cooling effectiveness studies of both adiabatic and conjugate cases.
- Study different kinds of film cooling holes shapes for adiabatic and conjugate film cooling effectiveness on convex surface of hot gas turbine components.
- Investigation for a new cooling hole scheme called heart-shaped and study its effect on mitigating the vortexes claimed to be responsible on lift-off phenomenon of conventional cooling holes.
- New conjugate blade technique called multi-layers has been investigated to be helpful in speeding up the heat absorption from the upper blade surface which is expose to the hot gas in gas turbine.

1.6 Overview of the thesis

In this thesis five chapters have been included and the contents of the chapters are summarized as follow:

Chapter one, the introduction, provides the fundamentals of film cooling technique in addition to mathematical background for film cooling effectiveness and heat transfer. Also the significance of computational fluid dynamic in film cooling studies has been presented.

Chapter two, the literature review, has been allocated to present the past studies on film cooling technique. The effect of the film cooling hole geometries, blade curvature, physical parameters and some other factors on the film cooling performance have been presented.

Chapter three, the methodology, includes the discussion for the computational domains, generation of cooling hole geometries, meshing independence procedure, and the boundary conditions of the studies. Also the turbulent model has been presented.

Chapter four, result and discussion, is the major chapter in this thesis which presents the finding of the investigations and studies that performed through on this work. Grid independence and validation study has been discussed. Also the effect of different kinds of cooling hole geometry on film cooling effectiveness has been discussed for both adiabatic and conjugate cases. In addition, the result of multi-layers technique is presented and discussed.

Chapter five, conclusion and recommendations, consist of the conclusions that come up based on the finding of this work in addition to recommendations for future studies.

CHAPTER 2

LITERATURE REVIEW

2.1 Introduction

Since film cooling performance is influenced by various physical and geometrical parameters further than the mutual effects for these parameters, film cooling is still under study and investigation. Because of the relatively low cost and high precision, computational fluid dynamics plays an important role in this part.

2.2 Effect of film cooling geometry on film cooling effectiveness, η

Over the past years cylindrical film cooling holes have been intensively investigated. Measurements in terms of effectiveness and heat transfer coefficients were presented including (Yuen et al., part I and part II, 2003, Yuen et al., part I and part II, 2005), and some analytical studies to understand the film cooling physics (Walters and Leylek, 2000). Some other studies aimed to improve the performance of cylindrical cooling holes by different arrangements such as double-jet ejection (Kusterer et al., 2007) or testing the effect of film hole row location on film cooling effectiveness (Jiang and Han, 1996). Shaped film cooling holes have become an overriding geometry in the film cooling studies due to their superior performance compared to traditional cylindrical cooling holes making them more effective both aerodynamically and thermally (Lee^a et al., 2002, Miao and Wu, 2006, Lu et al., 2007, Colban and Thole, 2007). Kim and Kim, 2004 conducted an experimental investigation for different shaped injection holes for the turbine blade leading edge film cooling, as shown in Figure 2.1. Different blowing ratios of 0.7, 1.0, 1.3 and 1.7 were used. In addition, the mainstream Reynolds number based on the cylindrical diameter was 7.1×10^4 .

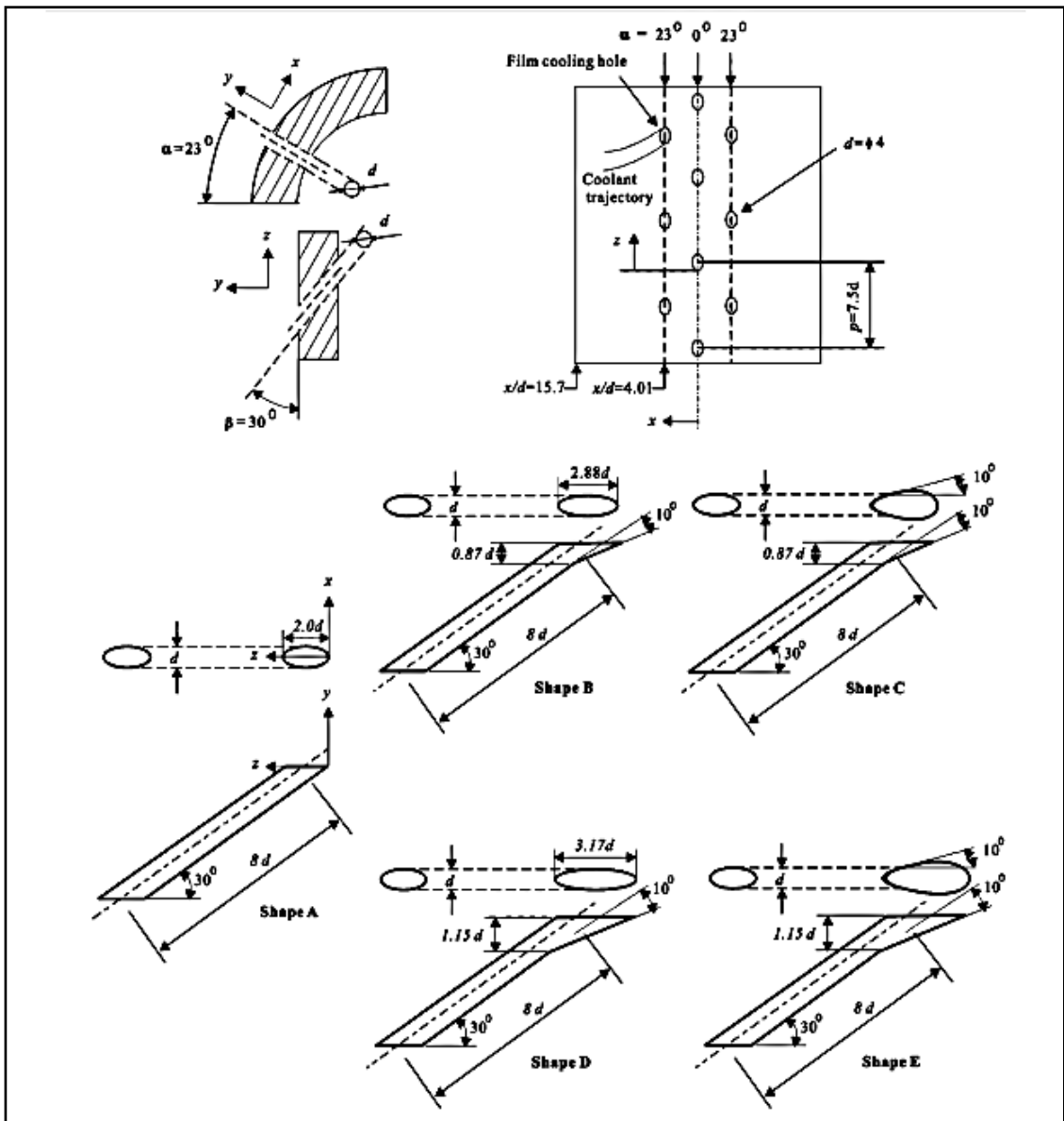


Figure 2.1: Overview of hole geometries and coordinate system (Kim and Kim, 2004).

The overall finding is that the shaped cooling holes were performed better than the cylindrical holes. Besides, shape D showed better film cooling effectiveness among the other shapes for all blowing ratios.

Bernier et al., 2009 investigated five different film cooling hole geometries, namely cylindrical (CYL), cylindrical trrenched (CYLT), fan (FAN), fan trrenched (FANT), and fan with a 30° injection angle with respect to the freestream velocity (FANA). Laterally average effectiveness, maximum effectiveness and film cooling uniformity coefficient

(CUC) were investigated. The cooling hole inclination angle was 35° . The investigation was performed for a range of blowing ratio from 0.5 to 2.0. The main finding is that at high blowing ratio, the FAN, FANT, and FANA hole geometries showed higher laterally averaged and maximum effectiveness compared to CYL for low X/D. However, The FANT and FANA exhibited a steady decrease in the laterally averaged and maximum effectiveness as X/D increases as illustrated in Figures 2.2 and 2.3.

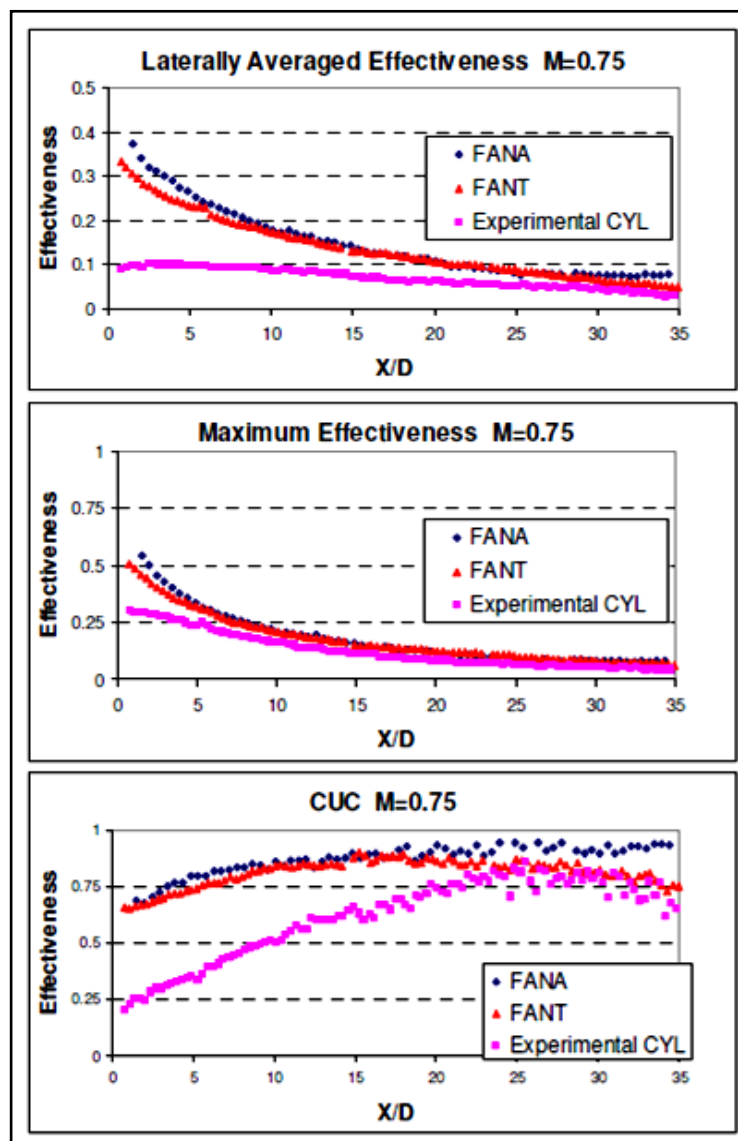


Figure 2.2: Experimental data comparison between the CYL, FANA and FANT for $M=0.75$ (Bernier et al., 2009).

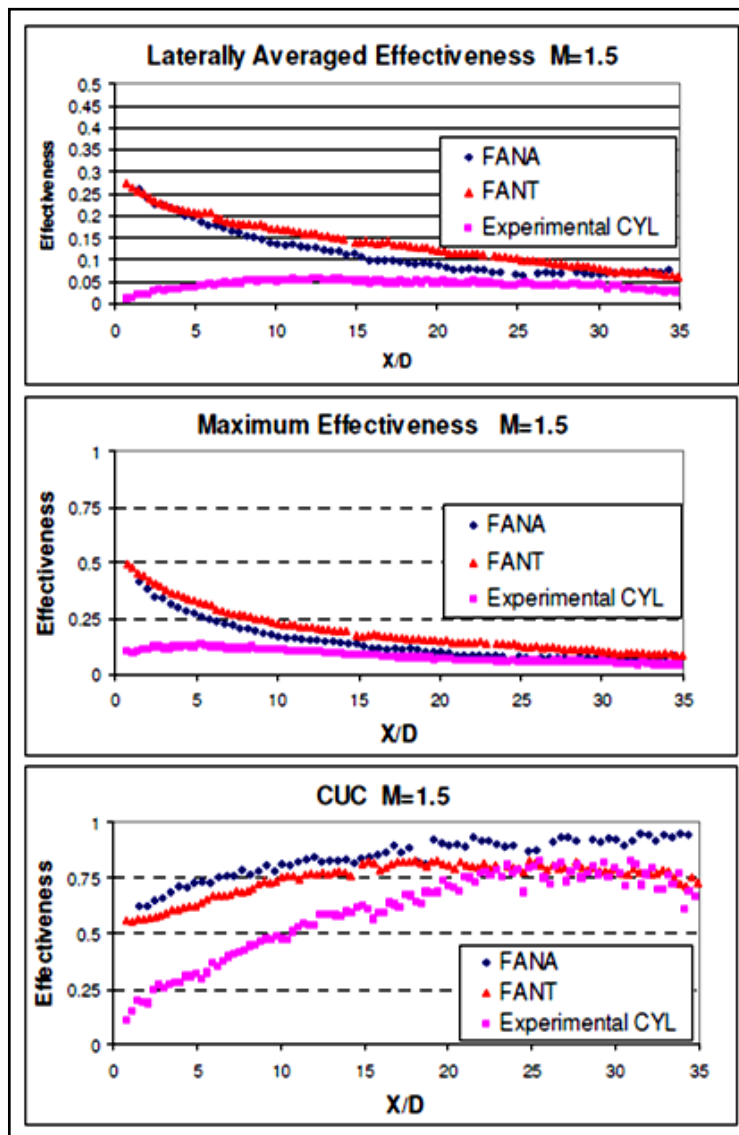


Figure 2.3: Experimental data comparison between the CYL, FANA and FANT for $M = 1.5$ (Bernier et al., 2009).

Ghorab et al., 2011 conducted an experimental investigation of film cooling performance of a louver scheme which is illustrated in Figure 2.4. Thermochromic liquid crystal technique was used. The investigation has been performed for blowing ratios from 0.5 to 1.5. The density ratio was 0.94. Their finding showed that the louver scheme has superior centerline and lateral film cooling effectiveness than other film cooling schemes referred in their study for comparison.

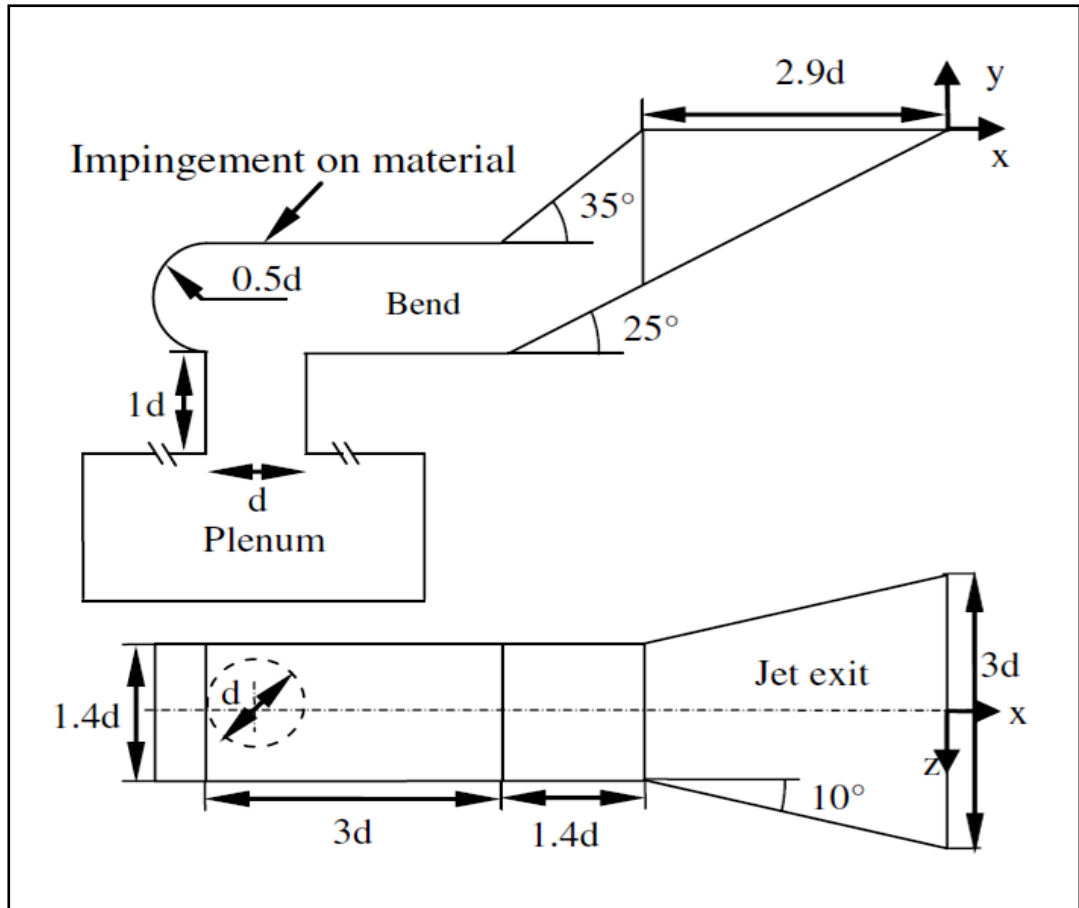


Figure 2.4: Louver film hole geometry (Ghorab et al., 2011).

Lee and Kim, 2011 numerically optimized a laidback fan-shaped film cooling hole as illustrated in Figures 2.5 and 2.6. Their work has been performed to evaluate the effects of geometric variables of laidback fan-shape hole on film cooling performance. They evaluated the effects of injection angle of the hole, the lateral expansion angle of the diffuser, the forward expansion angle of the hole and the ratio of the length to the diameter of the hole on the film cooling effectiveness. They found that an increase of the forward expansion angle makes a reduction of film cooling effectiveness. Also, lateral expansion angle has the biggest impact among the four geometrical variables on the spatially averaged film cooling effectiveness.

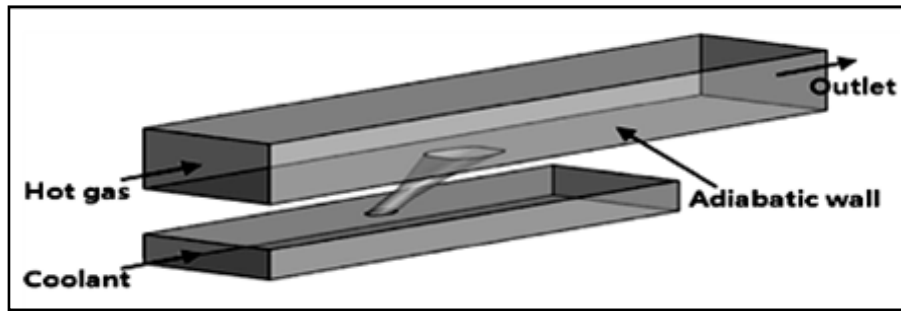


Figure 2.5: Computational domain (Lee and Kim 2011).

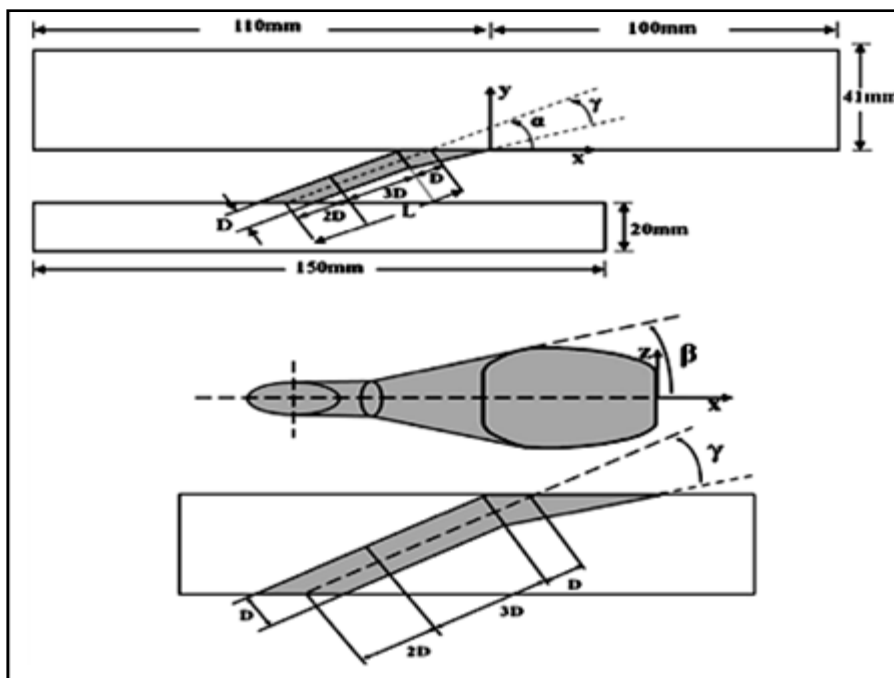


Figure 2.6: Geometrical parameters (Lee and Kim 2011).

Heneka et al., 2012 performed an experiment to investigate the film cooling effectiveness of laid-back fan-shaped holes. The study was carried out on a flat plate over a range of blowing ratio from $M = 0.5$ to $M = 3$ as shown in Figure 2.7. A variety of geometric parameters were tested, such as inclination angle, compound angle, area ratio, and pitch to diameter ratio. The result generally presented in term of adiabatic film cooling effectiveness. The finding indicated that increasing the area ratio and the compound angle cause greater effectiveness.

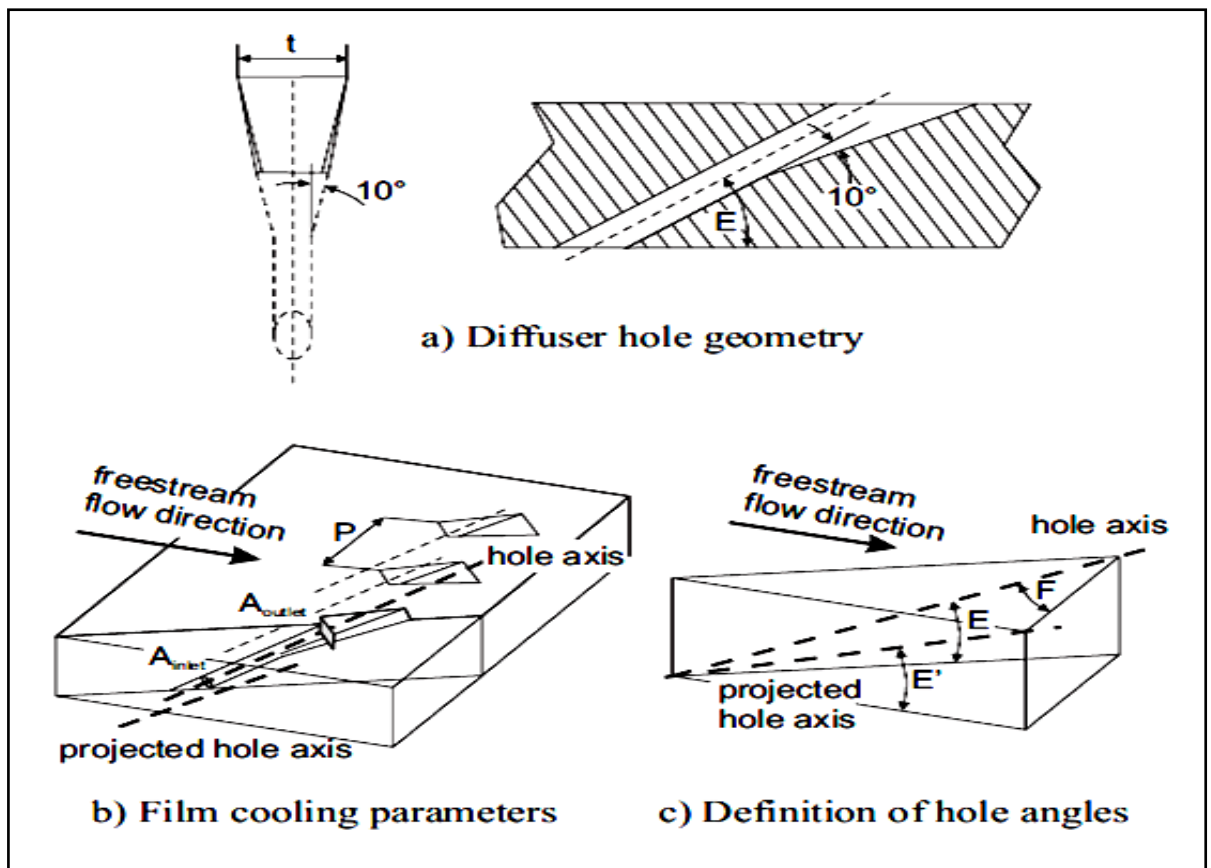


Figure 2.7: Definition of geometrical parameters (Heneka et al., 2012).

Guangchao et al., 2008 studied film cooling effectiveness and heat load h/h_o for the injection through cylindrical holes, 3-in-1 holes and fanned holes downstream of a row of holes with 45° inclination and 3 hole spacing apart. Figure 2.8 illustrates the geometries of the three film cooling holes. The outlet of fanned holes has a lateral expansion while in 3-in-1 case both inlet and outlet have lateral expansion. They applied CO_2 for secondary injection. Their study outlined that h/h_o of the cylindrical holes is highest and the h/h_o of the fanned holes is lowest for the injection through the holes with the three shapes and provide best film cooling performance among the three geometries.

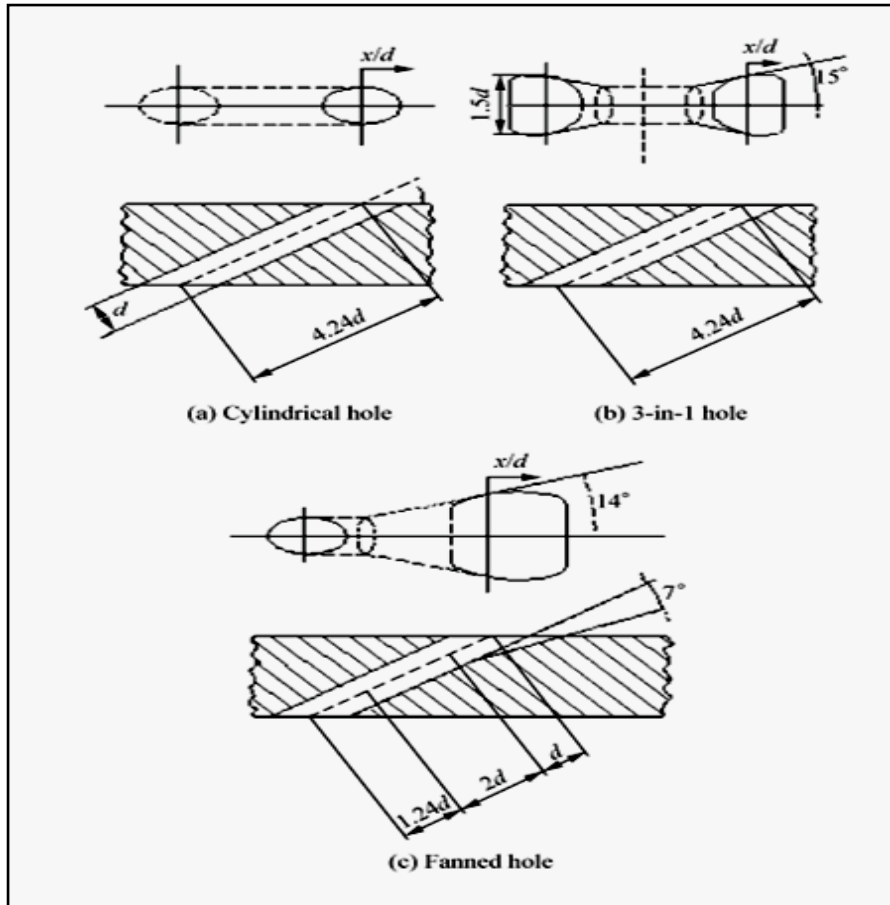


Figure 2.8: Geometries of three film cooling holes (Guangchao et al., 2008).

Black et al., 2011 investigated several slot-like film cooling designs on the suction side of turbine vane. The investigation included discrete and continuous slots as shown in Figure 2.9. Slot width varying and diffusing the coolant flow within the slot before emitting onto the test surface were considered. Their result indicated that as the widths decrease, continuous slots show a linear increase in spatially average adiabatic film cooling effectiveness for blowing ratios at or above $M=1.8$.



Figure 2.9: Top view of the continuous and discrete partial slot configurations (Black et al., 2011).

Islami et al., 2008 conducted computational study for a row of coolant injection holes on each side of a symmetrical turbine blade model near the leading edge. Four different holes configurations, a cylindrical, a forward diffused, a cylindrical within a transverse slot and forward diffused within a transverse slot were employed. They found that the shape of the hole and the integration of the holes with a continuous slot, significantly affect the film cooling flow over the protected surface. Bunker 2011 conducted an experiment of mesh-fed slot film cooling on a flat plate. The mesh-fed geometries composed of pedestal arrays with height to diameter ratios of 0.2 exiting onto 20° inclines to the surface. The result demonstrated that the mesh-fed film cooling effectiveness outperformed shaped diffuser holes but less than that of a more idealistic two dimensional slot film cooling geometry.

Horbach et al., 2011 performed an experimental study on trailing edge film cooling turbine blade using coolant ejection through planar slots on a pressure side cutback. The blowing ratio was varied at $0.2 < M < 1.25$. Different designs of the coolant ejection lip were studied and concluded that film cooling effectiveness influenced by ejection lip thickness.

Barigozzi ^a et al., 2012 carried out experimental investigation for the effects of the application of trenched cooling holes on film cooling in the front part of a contoured high pressure vane endwall. Two trench depth, shallow trench of depth 1.0D, where D is the hole diameter, and deeper trench of depth 1.2D were tested. Film cooling effectiveness investigation was performed using thermochromic liquid crystal technique. The study was performed at low isentropic Mach number of 0.2. In addition, low inlet turbulence intensity, namely 1% was utilized.

The main finding is that trenched holes are able to provide higher global film cooling effectiveness compared to the cylindrical cooling holes. However large amount of the coolant injection is required in trenched case. As for the trench depths, the shallow trench of depth 1.0D shows slightly higher effectiveness for mass flow rate ratio up to 0.83%. However, for the larger injection rates, the deeper trench of depth 1.2D is performed better. On the other hand, Tran et al., 2010 studied the effect of a rectangular mask on film cooling. The geometry was called masked film cooling or crater film cooling. Simple cylinder film cooling holes with inclination angle of 35° were used. Trench cooling hole was used for comparison. They found that the position of the crater relative to the cooling hole is significant. However, the trench cooling hole outperforms crater film cooling.

Kanani et al., 2008 numerically studied laterally diffused angle hole and a comparison with simple cylinder hole was performed. The blowing ratio ranged from 0.5 to 1.67 and the study has been carried out on a flat plate. They demonstrated that the film cooling effectiveness is influenced by the shape of the cooling hole.

Wright et al., 2011 studied the effect of density ratio on flat plate film cooling using pressure sensitive paint (PSP) technique. Three separated flat plates containing either simple cylinder holes, fan-shaped hole or laidback fan-shaped holes have been considered as shown in Figure 2.10. The blowing ratio range was $M = 0.25-2.0$ and the freestream turbulence intensity range was $Tu = 1-12.5\%$. The main finding of their study is that in all cases, as the freestream turbulence intensity increases, the film cooling effectiveness decreases. However, this effect is reduced as the blowing ratio increases for all three film cooling hole configurations.